

# ProCST: Boosting Semantic Segmentation using Progressive Cyclic Style-Transfer

Shahaf Etteedgui, Shady Abu-Hussein, and Raja Giryes

Tel Aviv University

**Abstract.** Using synthetic data for training neural networks that achieve good performance on real-world data is an important task as it has the potential to reduce the need for costly data annotation. Yet, a network that is trained on synthetic data alone does not perform well on real data due to the domain gap between the two. Reducing this gap, also known as domain adaptation, has been widely studied in recent years. In the unsupervised domain adaptation (UDA) framework, unlabeled real data is used during training with labeled synthetic data to obtain a neural network that performs well on real data. In this work, we focus on image data. Many UDA methods rely on transferring the style of the synthetic (source) data to be as similar as possible to the real (target) data either in the image or the feature domain. For the semantic segmentation task, it has been shown that performing image-to-image translation from source to target, and then training a network for segmentation on source annotations - leads to poor results. Therefore a joint training of both is essential, which has been a common practice in many techniques. Yet, closing the large domain gap between the source and the target by directly performing the adaptation between the two is challenging. In this work, we propose a novel two-stage framework for improving domain adaptation techniques. In the first step, we progressively train a multi-scale neural network to perform an initial transfer between the source data to the target data. We denote the new transformed data as “Source in Target” (SiT). Then, we use the generated SiT data as the input to any standard UDA approach. This new data has a reduced domain gap from the desired target domain, and the applied UDA approach further closes the gap. We demonstrate the improvement achieved by our framework with two state-of-the-art methods for semantic segmentation, DAFormer and ProDA, on two UDA tasks, GTA5 to Cityscapes and Synthia to Cityscapes. Code and state-of-the-art checkpoints of ProCST+DAFormer are provided in <https://github.com/shahaf1313/ProCST>.

**Keywords:** Image-to-image translation, Domain adaptation, Semantic segmentation

## 1 Introduction

In the semantic segmentation task, the goal is to output a segmentation map: an annotation of each pixel within a given image from a predetermined classes

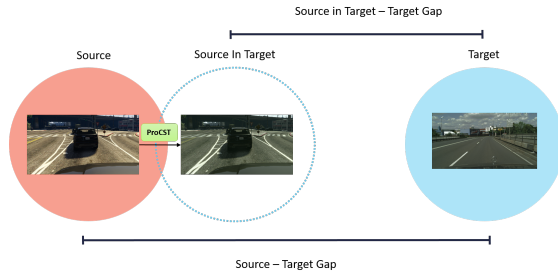


Fig. 1: Domain Gap Reduction using SiT images: Images from the source domain are translated onto a SiT domain, using our Progressive Cyclic Style-Transfer (ProCST) approach. The translated image preserves the content of the source image, but changes the appearance and style to the target domain’s appearance and style. This reduces the domain gap and thus helps UDA methods to learn improved semantic segmentation models for the target domain. The dashed blue line illustrates the reduced domain gap that ProCST achieves.

set. Over the past years, many deep learning-based approaches have been proposed for solving the semantic segmentation task. However, similarly to most deep learning approaches, a large amount of data is required to perform and generalize well. In some applications, such as classification, acquiring large annotated datasets can be relatively simple. Yet for semantic segmentation, where one needs to annotate every pixel, the task is very time-consuming and sometimes may include inaccuracies due to human error.

Unsupervised Domain Adaptation (UDA) aims at mitigating this lack of annotated training data. This area of research focuses on utilizing the vast amount of annotated data in a given source domain to infer the labels in a given target domain despite the fact that the target data lacks annotations. The most common source datasets are synthetic simulation data that contains class label annotations ‘for free’, and the target is real data that contain the same object classes as in the simulation.

The naive way of training a segmentation network only on source images and annotations fails to achieve good results because of the major differences between real-world images and synthetic images generated by the simulation [13]. Using the available images and annotations in order to decrease this domain gap is at the heart of UDA.

Different UDA techniques have been used to achieve good performance in the segmentation of the target domain. In these approaches, the real-world data, which do not have target segmentation maps, is incorporated together with the synthetic images and their annotations during training of the deep neural network that segments its input target images. For example, some suggested training a neural network using the annotated samples from the source domain, then either adapt the network to the target domain [44] or, alternatively, transfer the samples of the source domain to the target while preserving the structure of the



source images, such that the segmentation maps of the source can be used for the transferred images as labels [21, 34, 40].

These and most of the current methods try to close the entire domain gap at once. In this work, we offer a prior step to these methods, whose goal is to reduce the gap between the domains. This idea is depicted in Figure 1. We suggest Progressive Cyclic Style-Transfer (ProCST) network, which has a multi-scale architecture that uses progressive training for performing style transfer. In addition, this model uses the annotations of the source domain to preserve the semantic information in the transfer. Figure 2 presents the architecture of our method. ProCST narrows the domain gap between the source and the target domains, by translating the source images to mimic images from the target domain, which we refer to as “SiT”. The SiT dataset is closer to the target domain and preserves the images content. Hence, we use it instead of the source domain data as input to state-of-the-art UDA methods for semantic segmentation and show that it improves their performance. Figure 1 illustrates our proposed solution.

We evaluate our method on the UDA for semantic segmentation task, where the target domain in both cases is Cityscapes [4], and the source domains are either GTA5 [27] or Synthia [28]. We demonstrate the effectiveness of our scheme with two state-of-the-art methods for UDA semantic segmentation, ProDA [44] and DAFormer [14]. We calculate Mean Intersection Over Union [mIoU] over the test data of Cityscapes, and show improvement over these approaches and other well-known UDA techniques. For example, we get an improvement of 1.5% mIoU on GTA5 dataset (using our runs) over the DAFormer, which is the current state-of-the-art UDA approach. This demonstrates the effectiveness of our proposed framework.

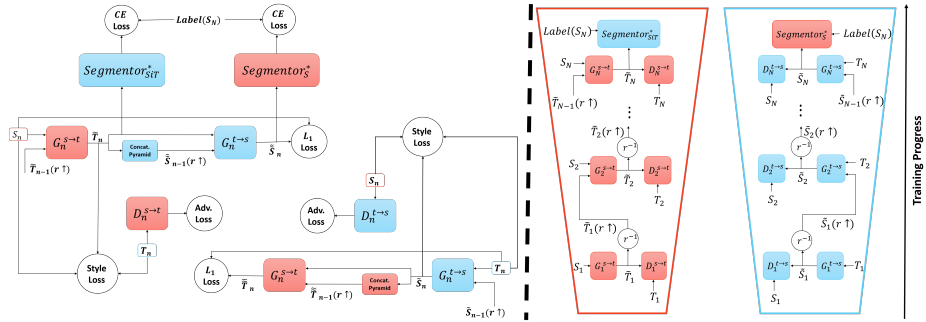


Fig. 2: ProCST model. Networks are colored by input domain: red for source domain and blue for target domain. On the right, the bi-directional multiscale image pyramid structure:  $\mathbb{S} \rightarrow \mathbb{T}$  and  $\mathbb{T} \rightarrow \mathbb{S}$  image translation. On the left, loss flowchart including all losses in the pyramid: for  $n \leq N$ , Cyclic Style Transfer loss. \*For  $n = N$ , additional label loss. More details appear in Section 3.

## 2 Related Work

*Semantic Segmentation* has been examined widely using deep learning methods [3, 23, 42, 46]. These methods propose different architectures and train them on pixel-wise manually annotated datasets such as Cityscapes [4]. However, the annotation procedure is time-consuming. Thus, it is hard to collect a large enough dataset of annotated images. In addition, training those architectures using small datasets usually leads to poor segmentation quality. One popular way to overcome this limitation is to train the network on synthetic data, where the annotations are available generously. Examples for synthetic data include GTA5 [27] and Synthia [28] datasets. Yet, due to the domain gap between the synthetic and the real data, the resulting model does not generalize well on the latter.

*Unsupervised Domain Adaptation* methods seek to align the two domain distributions [7, 13, 35, 38, 45]. The works of [9, 24, 43] adapt the source domain to the target domain by minimizing discrepancy measures and matching the statistical moments of the two domains. Yet, these methods struggle to translate the source domain appropriately, which leads to poor generalization over the target domain.

In [40] they approach the UDA task in a heuristic fashion, where they assume that the source domain can be adapted by solely swapping the lower frequencies of the two domains while preserving the higher frequencies that contain more relevant information for segmentation. However, such an approach works only when indeed the domain gap lies in the swapped frequencies. Moreover, this approach requires finding the specific swapping frequencies.

Another popular technique in domain adaptation is *Adversarial Learning* [6, 20, 30, 32], where a discriminator is trained to distinguish between target domain images and translated source domain images, while the translator (generator) tries to fool the discriminator. As a result, the generator learns to map the source images to the target domain. In [26] for instance, they utilize buffers from the simulator used to create the synthetic images for guiding the translation network to generate better looking images. This technique outputs good image quality but it fails to preserve image content, and thus preforms poorly when incorporated within a semantic segmentation framework as we show in Section 4.2.

Due to the nature of adversarial optimization schemes, the training process is not stable and therefore convergence is not guaranteed. Over the past decade, there have been many works that tried to stabilize adversarial learning [1, 2]. For domain adaptation, one successful training strategy is the addition of cyclic loss to the total objective [13, 41, 47], where each source image is translated to the target domain and then translated back to the source domain, where traditional  $\ell_p$  norm can be applied. A similar process is applied also on the target domain for the inverse direction. Since the cyclic loss uses standard norms, training tends to be much more stable than relying entirely on the adversarial loss term. Nevertheless, applying this approach solely in UDA for the task of semantic segmentation results in poor performance, since it fails to utilize the labels information.

For traditional Generative Adversarial Network (GANs) [10], one major step that enabled a high-resolution image generation was proposed by [16]. In this work, they suggest training the networks progressively. The proposed training procedure first trains the network to generate low-resolution images, then add layers to the network and increase the size of the generated images sequentially. This concept enabled the generation of high resolution images with superior quality, which since then has been followed by many works [16–19, 29, 37].

Other methods decrease the domain gap using Self-Supervised Learning (SSL) [14, 40, 44]. For instance, the work in [44] uses pseudo label denoising and target structure learning in a three stage training process that relies on denoising using prototypical class labels. In [14], they base their network architecture on two vision transformers [5, 22], where one is given a random augmentation of a random domain-mixed image, and is trained to map it to the source segmentation map in addition to the pseudo labels map of a teacher network, which accumulates the knowledge obtained through the training steps. Those methods perform well on the UDA semantic segmentation task, but the large domain gap limits their performance. Our framework generates SiT images that have smaller domain gap from the target dataset and thus applying the above UDA methods in combination with our framework results in upgraded performance.

In this paper, we propose a novel progressive multiscale cyclic style-based approach. Namely, a multiscale network is progressively trained in a cyclic fashion, with a style-based loss, conditioned on the segmentation maps of the source domain. We also add our novel Label Loss term, which as shown in the ablation section 4.3, is crucial for upgrading segmentation performance on target domain. After convergence, the source dataset is translated to mimic the target domain, while preserving the content of the original images for maintaining their pixel-wise correspondence with the segmentation maps. We refer to the new dataset as SiT (Source in Target) dataset, which is then used as the input source dataset when training state-of-the-art UDA methods. As shown in section 4, this process indeed improves their performance.

### 3 Method

We present ProCST, an image to image translation framework used as a zero-step before applying UDA methods and thus improve their performance. ProCST is a multiscale network trained with cyclic style transfer loss using a progressive training scheme. The model is composed of two main components: multiscale training and bi-directional image-to-image style translation. In addition, when training full resolution images we add two semantic segmentation networks that utilize source domain labels in the training procedure.

Our multiscale training is based on an image pyramid structure: a list of generators that creates a full scale translated image, where each generator is responsible for translating the image at a certain scale. The generator has two inputs: the first is a translated image from the generator of the previous scale, upsampled to the current scale size. The second is a resized version of the original

source image that matches the current generator scale. Note that the generator of the lowest scale receives only the second input. The output of each generator is a translated image in the scale it is using. This process is depicted in Figure 2.

Each scale consists of two generators:  $G^{st}$  for translating images from the source domain to the target domain, and  $G^{ts}$  for the inverse translation. Each of the generators has a separate discriminator,  $D^{st}$  and  $D^{ts}$ , respectively. Both the generators and the discriminators are CNNs with depth that increases with the resolution. A similar approach has been used to train a GAN using a single image for the task of image generation that receives noise and outputs an image [29], which is very different from the translation task of our method that transfers an image from one domain to another.

The training process is progressive in the sense that when the multiscale model is trained, the loss is affecting only the top scale and is not propagated to the lower scales. This training technique has proven to create realistic and clean images, as shown for the Progressive GAN [16], which is used for image generation (and not translation as we do here).

The losses in the progressive training process are a combination of the adversarial-cyclic-style criteria described in Section 3.3, which allow changing the visual style of the image but also preserving the original content. In addition, when training the full resolution image generators, we incorporate the cyclic label loss term, as detailed in Section 3.4. Before describing the loss functions, we start with some basic definitions that are used to describe our model.

### 3.1 Model Definitions

Let  $\mathbb{S}$  be the source domain, and  $\mathcal{S}$  be the source dataset with images  $s^{(l)}$  and annotations  $Label(s^{(l)})$ ,

$$\begin{aligned}\mathbb{S} &\subset \mathbb{R}^{H_S \times W_S \times 3} \times \mathbb{R}^{H_S \times W_S \times K} \\ \mathcal{S} &= \{(s^{(l)}, Label(s^{(l)})) \in \mathbb{S}\}_{l=0}^{N_S},\end{aligned}\tag{1}$$

where  $H_S, W_S$  are the height and width of source domain images,  $K$  is the number of class categories and  $N_S$  is the number of data points in the source dataset. In addition, let  $\mathbb{T}$  be the target domain, and  $\mathcal{T}$  be the target dataset with images  $t^{(l)}$ ,

$$\begin{aligned}\mathbb{T} &\subset \mathbb{R}^{H_T \times W_T \times 3} \\ \mathcal{T} &= \{t^{(l)} \in \mathbb{T}\}_{l=0}^{N_T},\end{aligned}\tag{2}$$

where  $H_T, W_T$  are the height and width of target domain images, and  $N_T$  is the number of data points in the source dataset.. Notice that the target domain annotations are not available, and we assume that source and target datasets share the same class categories,  $c = 1, \dots, K$ . Denote  $N$  the number of scales in the multiscale model of size  $N$ , and denote by  $0 < r < 1$  the scale factor between two adjacent scales. Then, at scale  $n$ , the dimensions are  $(H_n, W_n) = (r^{N-n}H_N, r^{N-n}W_N)$ , where  $H_n$  and  $W_n$  are the height and width of the images at scale  $n$ .

### 3.2 Model Architecture

ProCST that is presented in Figure 2 is a multiscale model. Scales are trained sequentially in a progressive training process. Each scale has two generators,  $G_n^{st}$  and  $G_n^{ts}$  and two discriminators,  $D_n^{st}$  and  $D_n^{ts}$ , where  $n$  denotes the scale level. We describe next the  $\mathbb{S} \rightarrow \mathbb{T}$  translation process, where the complementary translation  $\mathbb{T} \rightarrow \mathbb{S}$  is symmetric up to the last (highest) scale. In that scale, the source labels are also used for the label loss, which is described in Section 3.4.

At the  $n$ th scale,  $n = 1, \dots, N$ , ProCST generates SiT fake images using the generator chain  $G_k^{st}, k \leq n$ . Each generator receives the upscaled output of the previous generator and the current source image resized to the current scale’s size. This process is repeated till we reach the last scale. More formally, let  $s \in \mathcal{S}$  be a source image, and  $t \in \mathcal{T}$  be a target image. Let  $s_n, t_n$  be the resized source and target images to scale  $n$ , respectively. A fake SiT image  $\tilde{t}_n$  is generated using  $n$  generators  $G_k^{st}, k \leq n$  by the following procedure:

$$\begin{cases} \tilde{t}_n = G_n^{st}[s_n, \tilde{t}_{n-1}(r \uparrow)] & n > 1 \\ \tilde{t}_1 = G_1^{st}[s_1] & n = 1, \end{cases} \quad (3)$$

where  $(r \uparrow)$  means the image is upscaled by a factor of  $r^{-1}$ . For instance, on the right-hand-side of Figure 2 we can see that the second scale receives an upscaled output image from the first generator together with the resized source image. Both images share the same size: the size of the second scale. After generating the SiT fake image, we can now calculate an adversarial loss term and a style loss term (both described in Section 3.3) using the fake SiT image, source image, and target image, as depicted on the left-hand-side of Figure 2. Remember that the loss is not propagating to any scale other than scale  $n$ .

For calculating the cyclic loss, we generate a fake source image from the fake target image. We calculate the fake target-in-source image by feeding the created fake SiT image to the  $G_k^{ts}, k \leq n$  generators chain. This allows calculating the cyclic loss between the original source and the resulting SiT-in-source image.

### 3.3 Cyclic Style Transfer Loss

We use three loss terms in the cyclic style transfer loss, which incorporate a unique training procedure as described in Figure 2. Without loss of generality, we will focus on the  $\mathbb{S} \rightarrow \mathbb{T}$  translation. The inverse direction is symmetric for this loss bundle. Recall that  $s_n, \tilde{t}_n$ , and  $t_n$  are defined in Section 3.2. The triplet  $(s_n, \tilde{t}_n, t_n)$  is used in order to calculate the following three loss terms:

**Adversarial Loss.** We train a discriminator for each scale,  $D_n^{st}$ . We use a full CNN discriminator, using the Wasserstein GAN loss with gradient penalty [11].  $D_n^{st}$  receives  $(\tilde{t}_n, t_n)$  as fake and real images, respectively. The loss is given by

$$\mathcal{L}_{adv}^{st} = \mathcal{L}_{adv}^{st}(\tilde{t}_n, t_n). \quad (4)$$

**Style Loss.** Our method focuses on generating an image taken from a source domain to have the content of the original image but the appearance and style



Fig. 3: Bi-directional GTA5  $\leftrightarrow$  Cityscapes image translation. Left to right: GTA5, SiT, Cityscapes, and “Target in Source” translated images.

of the target domain. To fulfill this task we incorporate the style transfer loss, shown in [8] and [15], which uses features of a pretrained VGG-19 network. In [8], they have shown that some features control the texture and the style and some control the visual content of the image. The offered loss calculates two matrices:

*Content features* -  $\ell_2$  norm between the content image’s features and the fake image’s features. In our work,  $s_n$  is the content image and  $\tilde{t}_n$  is the fake image.

*Style features* -  $\ell_2$  norm between a Gram matrix (correlation matrix) of the style image’s features and a Gram matrix of the fake image’s features. Following [15], a total variation regularization is also added to the loss. Thus, a Style Loss term is given by:

$$\begin{aligned} \mathcal{L}_{style}^{st} = & \lambda_{content} \mathcal{L}_{content}^{st}(s_n, \tilde{t}_n) \\ & + \lambda_{style, Gram} \mathcal{L}_{style, Gram}^{st}(t_n, \tilde{t}_n) + \lambda_{TV} \mathcal{L}_{TV}^{st}(\tilde{t}_n). \end{aligned} \quad (5)$$

**Cyclic Loss.** Cyclic training [47] is a well known strategy in domain adaptation [13]. The main property of the cyclic training regime is the ability to trace back any translated image to the original domain. This is done by calculating the  $\ell_1$  loss between the original source image and the same source image that is translated twice (using  $G_n^{st}$  followed by  $G_n^{ts}$ ), namely  $\|s_n - \tilde{\tilde{s}}_n\|_1$ , where  $\tilde{\tilde{s}}_n$  denotes the source image that is translated twice.

The cyclic transfer procedure in ProCST is not trivial. First, we generate  $\tilde{t}_n$  as described earlier in Section 3.2. Then, we use the generators chain  $G_k^{ts}, k \leq n$  with a new input image  $\tilde{t}_n$ , in order to output the result of the cycle  $\tilde{\tilde{s}}_n$ . Namely:

$$\begin{aligned} \tilde{\tilde{s}}_n = & G_n^{ts}[\tilde{t}_n, \tilde{\tilde{s}}_{n-1}(r \uparrow)], \\ \mathcal{L}_{cyclic}^{ss} = & \|s_n - \tilde{\tilde{s}}_n\|_1. \end{aligned} \quad (6)$$

The above loss terms are unified to one Cyclic Style Transfer loss term

$$\begin{aligned}\mathcal{L}_{CST} &= \lambda_{adv} \mathcal{L}_{adv.} + \lambda_{style} \mathcal{L}_{style} + \lambda_{cyclic} \mathcal{L}_{cyclic} \\ &= \lambda_{adv.} (\mathcal{L}_{adv.}^{st} + \mathcal{L}_{adv.}^{ts}) + \lambda_{style} (\mathcal{L}_{style}^{st} + \mathcal{L}_{style}^{ts}) \\ &\quad + \lambda_{cyclic} (\mathcal{L}_{cyclic}^{ss} + \mathcal{L}_{cyclic}^{tt}),\end{aligned}\tag{7}$$

which is evaluated only at the current scale  $n$  in a progressive manner.

### 3.4 Label Loss

High resolution images contain a vast amount of knowledge and details. Generating good translation requires fine tuning and as much information as possible. We use the labels of the source dataset in order to better adapt to the new domain when more and more details become present. Adding a segmentation loss to image generation networks has proven to be effective, as can be seen at [26]. Thus, at the last scale of ProCST, we also use a label loss in addition to the losses in Section 3.3 that are used also in the lower scales. This is the only loss in our model that is not symmetric, i.e., it is not used in the  $T \rightarrow S$  direction.

The label loss has two different parts. The first consists of a segmentation network that is trained to segment SiT images,  $Segmentor_{SiT}$ . The input to this network is a SiT image, together with the segmentation map of the original source image. The second part is the novel cyclic label loss. We pretrained a segmentation network on the source dataset, as source annotations are available. Denote this pretrained network as  $Segmentor_S$ . We take the source image after it has been transferred using the cyclic operation from source to target and then back to source, and enter it to the pretrained  $Segmentor_S$  together with the original source segmentation map. This process results in a segmentation loss transfer between  $G^{st}$  and  $G^{ts}$ , which further encourages good segmentation features in both generators.

Each Segmentor network is trained with the well known Cross Entropy (CE) loss that is calculated between the segmentor’s output and the matching Ground Truth (GT) segmentation map. The CE loss between the prediction probability map  $p^{i,j,k} \in \mathbb{R}^{H \times W \times K}$  and segmentation map  $m^{i,j,k} \in \mathbb{R}^{H \times W \times K}$  is

$$\mathcal{L}_{CE}[p, m] = - \sum_{i=1}^H \sum_{j=1}^W \sum_{k=1}^K m^{i,j,k} \log p^{i,j,k}.\tag{8}$$

We use ResNet101 [12] as the segmentation network, which outputs a probability map per class. Input images to  $Segmentor_{SiT}$  are the translated SiT images and GT segmentation maps are the original source segmentation maps. Let  $Label(s_N)$  be the segmentation map of scale  $N$ , then the first part of the label loss is

$$\mathcal{L}_{CE, SiT} = \mathcal{L}_{CE}[Segmentor_{SiT}(\tilde{t}_N), Label(s_N)].\tag{9}$$





Fig. 4: Bi-directional Synthia  $\leftrightarrow$  Cityscapes image translation. Left to right: Synthia, SiT, Cityscapes, and “Target in Source” translated images.

This loss flows to the  $G_N^{st}$  generator and helps it distinguish both the class of the current pixel and the spatial distribution of each class in the source domain. Those properties help the translation process but also tend to improve segmentation properties of the translated SiT image.

In addition to the above network, we present our novel Cyclic Label Loss. Feeding both generators with segmentation loss will transfer the segmentation loss between domains. This property is very important to the UDA task, as the goal is good segmentation in the target domain. We denote the output of the cycle of source  $\rightarrow$  target  $\rightarrow$  source by  $\tilde{s}$ , which is a source domain image. As annotations from the source domain are available, we pretrained another ResNet101 on the source dataset, and used this pretrained *Segmentor<sub>S</sub>* as part of a loss for the cyclic  $\mathbb{S} \rightarrow \mathbb{T} \rightarrow \mathbb{S}$  loop. Specifically, our loss requires the segmentation map that is trained on the real source data to succeed also on  $\tilde{s}$ , i.e., the loss is given by

$$\mathcal{L}_{CE,ss} = \mathcal{L}_{CE}[\text{Segmentor}_S(\tilde{s}_N), \text{Label}(s_N)]. \quad (10)$$

This loss impacts both generators and acts as a segmentation information transporter between source and target domains.

The complete loss of scale  $n = N$  is composed of the loss terms in Section 3.3, in addition to the label losses presented above, i.e.,

$$\mathcal{L}_{last\_scale} = \mathcal{L}_{CST} + \lambda_{labels}(\mathcal{L}_{CE,sit} + \mathcal{L}_{CE,ss}). \quad (11)$$

### 3.5 Boosting Generic UDA Method

We turn to describe how ProCST can be used to improve existing UDA techniques. A generic UDA method takes as input a source dataset and a target dataset, and outputs segmentation maps of the target dataset, namely:

$$\text{UDA}[\mathcal{S}, \mathcal{T}] \rightarrow \text{Label}(\mathcal{T}). \quad (12)$$



Generic UDA methods encounter a large gap between the source and target domains. Training a ProCST model results in a chain of domain adapters,  $\{G_n^{st}, G_n^{ts}\}_{n=1}^N$ , that reduces this gap. Let  $\text{ProCST}_{\mathbb{S} \rightarrow \mathbb{T}}$  be a trained ProCST model that translates images from a source domain  $\mathbb{S}$  to images that mimic images from the target domain  $\mathbb{T}$ . We can build a new SiT dataset using this model, with the same annotation maps as the original source dataset:

$$\begin{aligned} \text{SiT} &= \{(\text{ProCST}_{\mathbb{S} \rightarrow \mathbb{T}}\{s\}, \text{Label}(s)), \forall s \in \mathcal{S}\}, \\ &= \{(\tilde{t}^{(l)}, \text{Label}(s^{(l)}))\}_{l=1}^{N_S}. \end{aligned} \quad (13)$$

The SiT is an in-between dataset, i.e., its domain gap from the desired target dataset is smaller than the original source dataset - as depicted in Figure 1. One may now train any arbitrary UDA method with the domain adapted SiT data:

$$\text{UDA}[\text{SiT}, \mathcal{T}] \rightarrow \text{Label}(\mathcal{T}). \quad (14)$$

In this way, the same UDA method encounters a smaller domain gap and thus achieves increased accuracy. This is a generic approach that boosts performance of UDA methods using a zero-step narrowing the domain gap.

## 4 Experiments

We turn to present the results of our proposed framework. We first describe the implementation details of the ProCST model and the creation of the SiT data. In addition, we show the results of integrating two robust UDA methods within our framework. We also provide a qualitative comparison between the images in the SiT data and the original source data and a quantitative comparison between the results achieved using ProCST SiT data and those achieved using data generated by another state-of-the-art image-to-image translation method. Moreover, we present an ablation study that demonstrates the importance of the different parts in the ProCST model. Finally, we discuss some of the limitations of ProCST. In Section 6 we present additional outputs of ProCST.

### 4.1 Implementation Details

**Datasets.** Source datasets: The GTA5 dataset [27] contains 24,966 images of size (1052, 1914) and their pixel-wise annotations. The Synthia dataset contains 9400 images of size (760, 1280) and their pixel-wise annotations.

Target dataset: The Cityscapes dataset [4], with the extra available train images: total of 22,973 images of size (1024, 2048).

Preprocessing of the source datasets includes two steps: first, we resize the input images to a size that preserves aspect ratio of the original source image. This size varies between domains (different domains have different image size and aspect ratio), but all domain resized images are larger than (512, 1024). Then, we take a random crop of size (512, 1024) from the resized images. The target

dataset has an aspect ratio of 1:2. Therefore, its preprocessing includes only resizing to (512, 1024), without any cropping. Thus,  $(H_N, W_N) = (512, 1024)$ .

**Network Architecture.** We use  $N = 3$  scales, with a scale factor  $r = 0.5$ . Generators and discriminators are fully convolutional, with width of 64 channels for all  $n$  and depth of 5 layers at scale  $n = 1$ , and 7 layers at scales  $n = 2, 3$ . For all generators and discriminators, we used a normalization according to the current scale’s batch size. Following [39], we normalized using Batch Normalization only if the number of images per GPU in the current scale exceeds 16. Otherwise, we used Group Normalization with groups number  $G = 8$ . We used DeepLabV2 [3] for both segmentation networks.

**Training.** We used the Adam optimizer for all generators and discriminators networks with parameters  $lr_g, lr_d = 0.0001$ . The optimizer for the segmentation networks is SGD with learning rate of  $lr_{semseg} = 0.0001$ . The weights of the losses were chosen to prefer style transfer, but if we would have discarded one of the other losses it would have caused either a dramatic performance degradation or a lack of model convergence, as can be seen in Table 3. We adopt the values of  $\lambda_{content}$ ,  $\lambda_{style, Gram}$  and  $\lambda_{TV}$  from [15]. To control the relative size of this loss compared to the other losses in ProCST, we normalized the maximum weight to 1 and kept the ratio between all other weights. The original values are  $\lambda_{content} = 1$ ,  $\lambda_{style, Gram} = 30$ ,  $\lambda_{TV} = 1$ . For  $\mathcal{L}_{CST}$  we set  $\lambda_{adv.} = 1$ ,  $\lambda_{style} = 10$ ,  $\lambda_{cyclic} = 1$ , and for the label loss we set  $\lambda_{labels} = 3$ .

**SiT Data Creation.** After training ProCST as described above, we generate the SiT data, where the input of the ProCST model are images from GTA5 or Synthia, and the output image are in Cityscapes style, as figures 3 and 4 show.

## 4.2 Results

We trained our model on two source datasets, GTA5 and Synthia, that were then translated to obtain the new SiT data (created per dataset). The data is used to train two state-of-the-art UDA methods, ProDA [44] and DAFormer [14].

Table 1 shows the results compared to other methods and also to the DAFormer and ProDA when trained with the regular source data. Notice that training ProDA using our SiT data resulted in an improvement of 1.1% mIoU over the original GTA5 dataset, and improvement of 0.6% mIoU over the original Synthia dataset. Training DAFormer using our SiT dataset achieved improvement of 1.5% mIoU over the original GTA5 dataset, and improvement of 1.1% mIoU over the original Synthia dataset. Note that the DAFormer results refer to our runs. The results of ProCST + DAFormer surpass current state-of-the-art results on both GTA5 and Synthia datasets.

Figure 3 emphasises the similarity between images from the SiT dataset, generated by ProCST, to images from the target dataset. The GTA5 dataset tries to simulate the view in the yellow and sunny Los Angeles, while the Cityscapes dataset was shot in the roads of the green and cloudy Germany. We can see how the ProCST model catches these differences and translates the yellow-red images of GTA5 onto images with blue-green atmosphere, while the translation in the opposite direction gives the image a red-yellow atmosphere.

Table 1: Comparison with state-of-the-art UDA methods for semantic segmentation. \*Average of 3 seeds, results using our runs.

	Road	S.walk	Build.	Wall	Fence	Pole	Light	Sign	Vege.	Terrain	Sky	Person	Rider	Car	Truck	Bus	Train	M.bike	Bike	mIoU
GTA5 → Cityscapes																				
CyCADA [13]	86.7	35.6	80.1	19.8	17.5	38.0	39.9	41.5	82.7	27.9	73.6	64.9	19.0	65.0	12.0	28.6	4.5	31.1	42.0	42.7
CBST [25]	91.8	53.5	80.5	32.7	21.0	34.0	28.9	20.4	83.9	34.2	80.9	53.1	24.0	82.7	30.3	35.9	16.0	25.9	42.8	45.9
FADA [33]	91.0	50.6	86.0	43.4	29.8	36.8	43.4	25.0	86.8	38.3	87.4	64.0	38.0	85.2	31.6	46.1	6.5	25.4	37.1	50.1
DACS [31]	89.9	39.7	87.9	30.7	39.5	38.5	46.4	52.8	88.0	44.0	88.8	67.2	35.8	84.5	45.7	50.2	0.0	27.3	34.0	52.1
CorDA [36]	94.7	63.1	87.6	30.7	40.6	40.2	47.8	51.6	87.6	47.0	89.7	66.7	35.9	90.2	48.9	57.5	0.0	39.8	56.0	56.6
ProDA [44]	87.8	56.0	79.7	<b>46.3</b>	44.8	45.6	53.5	53.5	88.6	45.2	<b>82.1</b>	70.7	<b>39.2</b>	88.8	45.5	<b>59.4</b>	<b>1.0</b>	48.9	56.4	57.5
ProDA + ProCST(ours)	<b>90.0</b>	<b>61.2</b>	<b>81.2</b>	40.8	<b>45.9</b>	<b>49.0</b>	<b>57.8</b>	<b>59.8</b>	<b>88.9</b>	<b>46.9</b>	80.1	<b>72.8</b>	34.6	<b>89.5</b>	<b>46.3</b>	58.7	0.0	<b>51.0</b>	<b>59.2</b>	<b>58.6</b>
DAFormer* [14]	94.9	64.2	89.4	53.6	45.7	48.8	55.8	61.5	90.0	<b>50.3</b>	91.9	71.5	43.8	92.0	73.0	77.0	67.6	55.9	63.4	67.9
DAFormer* + ProCST (ours)	<b>95.4</b>	<b>68.2</b>	<b>89.8</b>	<b>55.1</b>	<b>46.4</b>	<b>50.4</b>	<b>56.4</b>	<b>63.4</b>	<b>90.4</b>	49.9	<b>92.3</b>	<b>72.4</b>	<b>45.3</b>	<b>92.6</b>	<b>78.4</b>	<b>81.2</b>	<b>70.6</b>	<b>56.8</b>	<b>63.6</b>	<b>69.4</b>
Synthia → Cityscapes																				
CBST [25]	68.0	29.9	76.3	10.8	1.4	33.9	22.8	29.5	77.6	-	78.3	60.6	28.3	81.6	-	23.5	-	18.8	39.8	42.6
DACS [31]	80.6	25.1	81.9	21.5	2.9	37.2	22.7	24.0	83.7	-	90.8	67.6	38.3	82.9	-	38.9	-	28.5	47.6	48.3
CorDA [36]	93.3	61.6	85.3	19.6	5.1	37.8	36.6	42.8	84.9	-	90.4	69.7	41.8	85.6	-	38.4	-	32.6	53.9	55.0
ProDA [44]	87.8	45.7	84.6	<b>37.1</b>	0.6	44	54.6	37.0	<b>88.1</b>	-	84.4	<b>74.2</b>	24.3	88.2	-	51.1	-	<b>40.5</b>	<b>45.6</b>	55.5
ProDA + ProCST(ours)	87.8	<b>48.2</b>	<b>85.8</b>	22.9	<b>0.7</b>	<b>47.1</b>	<b>56.4</b>	<b>47.1</b>	88.0	-	<b>86.8</b>	72.4	<b>25.4</b>	<b>90.2</b>	-	<b>58.0</b>	-	38.3	41.9	<b>56.1</b>
DAFormer* [14]	<b>85.9</b>	<b>45.1</b>	<b>88.3</b>	39.0	<b>8.7</b>	49.8	54.2	52.4	86.2	-	87.0	72.5	47.7	86.5	-	49.0	-	52.6	62.5	60.5
DAFormer* + ProCST (ours)	84.8	39.5	88.2	<b>40.2</b>	7.3	<b>51.1</b>	<b>56.3</b>	<b>55.1</b>	<b>86.5</b>	-	<b>89.8</b>	<b>74.6</b>	<b>48.4</b>	86.5	-	<b>58.6</b>	-	<b>55.6</b>	<b>62.9</b>	<b>61.6</b>



Fig. 5: ProCST preserves source image content. On the left - original source image. In the middle, translated image from GTA5 to Cityscapes using EPE [26]. On the right - translated image from GTA5 to Cityscapes using ProCST. We can see that the tree in the red box disappears after EPE’s translation, but the translation of ProCST preserves the tree although it is surrounded entirely by sky.

In addition, we can see that ProCST changes appearance and textures to the desired dataset’s appearance and textures. The colors and textures of the road turn from rough yellow-grey in GTA5 to smooth gray, as in Cityscapes. The sky turns from clear blue to foggy and grey. The color of the vegetation turns from green-yellow into deep green. These changes appear also in the opposite translation. While the style and appearance of the images change, the visual content and details do not. This is an important property for UDA tasks, as annotations are available only on the original source dataset. Furthermore, we can see similar trends also in the Synthia to Cityscapes translation in Figure 4.

Other state of the art image to image translation methods lack content preservation property and thus do not achieve as good results on UDA tasks. For instance, we can see the difference between image translation of the state-of-the-art translation approach Enhancing Photorealism Enhancement (EPE) [26] and the image translation of ProCST in Figure 5. While EPE’s method has very good visual quality, it sometimes deletes some of the content of the original image, such as trees surrounded by sky background. The combination of cyclic loss together with style loss helps ProCST to change the style but yet preserve the content, which is a crucial property to the success in a generic UDA task. Although EPE’s translation performs well on image visual quality, it does not achieve good accuracy when used as a SiT data generator for UDA, as shown in Table 2. The results shown in this table use DAFormer as a baseline UDA method when trained on the SiT data generated by either ProCST or EPE. The published translated data of [26] contains only a subset of the original GTA5 dataset and a full pretrained model of EPE is not published. Therefore, for a fair comparison we trained DAFormer using the exact SiT subset generated by EPE also when using ProCST.

Table 2: Content Preservation of ProCST. Training DAFormer on different SiT data. Both rely on the exact subset of GTA5 published in [26].

Dataset	mIoU[%]
EPE [26]	61.9
ProCST	<b>67.3</b>

### 4.3 Ablation Study

We trained a ProCST model using 5 different configurations to find out what parts of the proposed architecture contribute most to the boost in performance. The examined parameters are the Multiscale Pyramid length (controlled by  $N$ ), Label Loss term (controlled by  $\lambda_{labels}$ ), Style Loss term (controlled by  $\lambda_{style}$ ) and Cyclic Loss term (controlled by  $\lambda_{cyclic}$ ). Each ablation discards one parameter, namely, set either number of levels  $N$  to 1 or the corresponding  $\lambda$  to 0.

We perform the ablation using the DAFormer on  $GTA5 \rightarrow Cityscapes$  with the SiT data as input and a minor hyper parameter tuning by changing DAFormer’s EMA update parameter to  $\alpha = 0.997$  from the original value of  $\alpha = 0.999$ . The reason for this tuning lays on the differences between the source and the SiT datasets. The original DAFormer method is optimized to the original source datasets. Thus, we fine-tuned its EMA update parameter to our new SiT dataset. For a complete and fair comparison, we also show the results of the DAFormer using the original GTA5 dataset as source with both values of  $\alpha$ .

Table 3 shows that if we omit either the style or cyclic loss terms, ProCST fails to converge. Moreover, omitting either the multiscale structure or label loss results in performance degradation compared to the full ProCST model. Note that we use just one (same) seed in the ablation (thus it is different than the one used in Table 1).

*Limitations.* We trained our model using a single NVIDIA RTX A6000. Memory usage is high due to the multiple losses involved in the training process and the high resolution of the input images. Training a full model may take 7-9 days,

but once it is done, the output SiT data can be used for multiple UDA tasks and does not require any adaptations per technique as we have shown here. Due to memory limitation we perform the image-to-image translation on a slightly lower resolution of the original images. We believe that the performance we achieve can be further improved if the translation would have been performed on the full resolution images.

Table 3: DAFormer [14] UDA method trained on different datasets. Training configuration on ProCST dataset is identical to DAFormer’s original configuration, excluding EMA update parameter that is set to  $\alpha = 0.997$ . Source dataset is trained with the original configuration and  $\alpha = 0.999$ .

\*Training with  $\alpha = 0.997$ .

Dataset	Label Loss	Multiscale Pyramid	Style Loss	Cyclic Loss	mIoU[%]	Relative[%]
Source					66.4	+0.0
Source*					66.3	-0.1
ProCST*	✓	✓	×	✓	×	×
	✓	✓	✓	×	×	×
	×	✓	✓	✓	67.2	+0.8
	✓	×	✓	✓	67.2	+0.8
	✓	✓	✓	✓	<b>68.2</b>	<b>+1.8</b>

## 5 Conclusion

In this work, we have shown a new concept that achieves improved performance of generic UDA methods. Our image to image translation method narrows the domain gap as a prior step to UDA training. ProCST translates source images to mimic the target domain but preserves the source images structure. We have shown that this improves the ProDA and DAFormer state-of-the-art UDA methods. To our knowledge, our cyclic label loss was not used before. From the examination we performed in this work, one can observe that this term regularizes the training and allows the model to achieve superior translation quality. We believe that this concept can be extended to other types of problems, where annotating images in a target domain of interest is very costly.

**Acknowledgment.** This research was supported by ERC-StG SPADE grant no. 757497. We would like to thank Deborah Cohen for her helpful comments.

## References

1. Arjovsky, M., Chintala, S., Bottou, L.: Wasserstein generative adversarial networks. In: International conference on machine learning. pp. 214–223. PMLR (2017)
2. Berthelot, D., Schumm, T., Metz, L.: Began: Boundary equilibrium generative adversarial networks. arXiv preprint arXiv:1703.10717 (2017)
3. Chen, L.C., Papandreou, G., Kokkinos, I., Murphy, K., Yuille, A.L.: Deeplab: Semantic image segmentation with deep convolutional nets, atrous convolution, and fully connected crfs. *IEEE transactions on pattern analysis and machine intelligence* **40**(4), 834–848 (2017)
4. Cordts, M., Omran, M., Ramos, S., Rehfeld, T., Enzweiler, M., Benenson, R., Franke, U., Roth, S., Schiele, B.: The cityscapes dataset for semantic urban scene understanding. In: Proceedings of the IEEE conference on computer vision and pattern recognition. pp. 3213–3223 (2016)
5. Dosovitskiy, A., Beyer, L., Kolesnikov, A., Weissenborn, D., Zhai, X., Unterthiner, T., Dehghani, M., Minderer, M., Heigold, G., Gelly, S., Uszkoreit, J., Houlsby, N.: An image is worth 16x16 words: Transformers for image recognition at scale. In: International Conference on Learning Representations (2021)
6. Ganin, Y., Lempitsky, V.: Unsupervised domain adaptation by backpropagation. In: International conference on machine learning. pp. 1180–1189. PMLR (2015)
7. Gao, L., Zhang, J., Zhang, L., Tao, D.: Dsp: Dual soft-paste for unsupervised domain adaptive semantic segmentation. In: Proceedings of the 29th ACM International Conference on Multimedia. pp. 2825–2833 (2021)
8. Gatys, L.A., Ecker, A.S., Bethge, M.: Image style transfer using convolutional neural networks. In: Proceedings of the IEEE conference on computer vision and pattern recognition. pp. 2414–2423 (2016)
9. Geng, B., Tao, D., Xu, C.: Daml: Domain adaptation metric learning. *IEEE Transactions on Image Processing* **20**(10), 2980–2989 (2011)
10. Goodfellow, I., Pouget-Abadie, J., Mirza, M., Xu, B., Warde-Farley, D., Ozair, S., Courville, A., Bengio, Y.: Generative adversarial nets. *Advances in neural information processing systems* **27** (2014)
11. Gulrajani, I., Ahmed, F., Arjovsky, M., Dumoulin, V., Courville, A.C.: Improved training of wasserstein gans. *Advances in neural information processing systems* **30** (2017)
12. He, K., Zhang, X., Ren, S., Sun, J.: Deep residual learning for image recognition. In: Proceedings of the IEEE conference on computer vision and pattern recognition. pp. 770–778 (2016)
13. Hoffman, J., Tzeng, E., Park, T., Zhu, J.Y., Isola, P., Saenko, K., Efros, A., Darrell, T.: Cycada: Cycle-consistent adversarial domain adaptation. In: International conference on machine learning. pp. 1989–1998. PMLR (2018)
14. Hoyer, L., Dai, D., Van Gool, L.: Daformer: Improving network architectures and training strategies for domain-adaptive semantic segmentation. arXiv preprint arXiv:2111.14887 (2021)
15. Johnson, J., Alahi, A., Fei-Fei, L.: Perceptual losses for real-time style transfer and super-resolution. In: European conference on computer vision. pp. 694–711. Springer (2016)
16. Karras, T., Aila, T., Laine, S., Lehtinen, J.: Progressive growing of gans for improved quality, stability, and variation. arXiv preprint arXiv:1710.10196 (2017)
17. Karras, T., Aittala, M., Hellsten, J., Laine, S., Lehtinen, J., Aila, T.: Training generative adversarial networks with limited data. *Advances in Neural Information Processing Systems* **33**, 12104–12114 (2020)

18. Karras, T., Aittala, M., Laine, S., Härkönen, E., Hellsten, J., Lehtinen, J., Aila, T.: Alias-free generative adversarial networks. *Advances in Neural Information Processing Systems* **34** (2021)
19. Karras, T., Laine, S., Aila, T.: A style-based generator architecture for generative adversarial networks. In: *Proceedings of the IEEE/CVF conference on computer vision and pattern recognition*. pp. 4401–4410 (2019)
20. Kumar, A., Sattigeri, P., Wadhawan, K., Karlinsky, L., Feris, R., Freeman, B., Wornell, G.: Co-regularized alignment for unsupervised domain adaptation. *Advances in Neural Information Processing Systems* **31** (2018)
21. Li, Y., Yuan, L., Vasconcelos, N.: Bidirectional learning for domain adaptation of semantic segmentation. In: *Proceedings of the IEEE/CVF Conference on Computer Vision and Pattern Recognition*. pp. 6936–6945 (2019)
22. Liang, J., Cao, J., Sun, G., Zhang, K., Van Gool, L., Timofte, R.: Swinir: Image restoration using swin transformer. In: *Proceedings of the IEEE/CVF International Conference on Computer Vision*. pp. 1833–1844 (2021)
23. Long, J., Shelhamer, E., Darrell, T.: Fully convolutional networks for semantic segmentation. In: *Proceedings of the IEEE conference on computer vision and pattern recognition*. pp. 3431–3440 (2015)
24. Mancini, M., Porzi, L., Bulò, S.R., Caputo, B., Ricci, E.: Boosting domain adaptation by discovering latent domains. In: *Proceedings of the IEEE Conference on Computer Vision and Pattern Recognition*. pp. 3771–3780 (2018)
25. Park, T., Liu, M.Y., Wang, T.C., Zhu, J.Y.: Semantic image synthesis with spatially-adaptive normalization. In: *Proceedings of the IEEE/CVF conference on computer vision and pattern recognition*. pp. 2337–2346 (2019)
26. Richter, S.R., AlHaija, H.A., Koltun, V.: Enhancing photorealism enhancement. *arXiv preprint arXiv:2105.04619* (2021)
27. Richter, S.R., Vineet, V., Roth, S., Koltun, V.: Playing for data: Ground truth from computer games. In: Leibe, B., Matas, J., Sebe, N., Welling, M. (eds.) *European Conference on Computer Vision (ECCV)*. LNCS, vol. 9906, pp. 102–118. Springer International Publishing (2016)
28. Ros, G., Sellart, L., Materzynska, J., Vazquez, D., Lopez, A.M.: The synthia dataset: A large collection of synthetic images for semantic segmentation of urban scenes. In: *Proceedings of the IEEE conference on computer vision and pattern recognition*. pp. 3234–3243 (2016)
29. Shaham, T.R., Dekel, T., Michaeli, T.: Singan: Learning a generative model from a single natural image. In: *Proceedings of the IEEE/CVF International Conference on Computer Vision*. pp. 4570–4580 (2019)
30. Shu, R., Bui, H.H., Narui, H., Ermon, S.: A DIRT-T approach to unsupervised domain adaptation. In: *6th International Conference on Learning Representations, ICLR* (2018)
31. Tranheden, W., Olsson, V., Pinto, J., Svensson, L.: Dacs: Domain adaptation via cross-domain mixed sampling. In: *Proceedings of the IEEE/CVF Winter Conference on Applications of Computer Vision*. pp. 1379–1389 (2021)
32. Tzeng, E., Hoffman, J., Saenko, K., Darrell, T.: Adversarial discriminative domain adaptation. In: *Proceedings of the IEEE conference on computer vision and pattern recognition*. pp. 7167–7176 (2017)
33. Wang, H., Shen, T., Zhang, W., Duan, L.Y., Mei, T.: Classes matter: A fine-grained adversarial approach to cross-domain semantic segmentation. In: *European conference on computer vision*. pp. 642–659. Springer (2020)

34. Wang, K., Yang, C., Betke, M.: Consistency regularization with high-dimensional nonadversarial source-guided perturbation for unsupervised domain adaptation in segmentation. In: AAAI (2021)
35. Wang, M., Deng, W.: Deep visual domain adaptation: A survey. *Neurocomputing* **312**, 135–153 (2018)
36. Wang, Q., Dai, D., Hoyer, L., Van Gool, L., Fink, O.: Domain adaptive semantic segmentation with self-supervised depth estimation. In: Proceedings of the IEEE/CVF International Conference on Computer Vision. pp. 8515–8525 (2021)
37. Wang, T.C., Liu, M.Y., Zhu, J.Y., Tao, A., Kautz, J., Catanzaro, B.: High-resolution image synthesis and semantic manipulation with conditional gans. In: Proceedings of the IEEE conference on computer vision and pattern recognition. pp. 8798–8807 (2018)
38. Wilson, G., Cook, D.J.: A survey of unsupervised deep domain adaptation. *ACM Trans. Intell. Syst. Technol.* **11**(5) (jul 2020)
39. Wu, Y., He, K.: Group normalization. In: Proceedings of the European conference on computer vision (ECCV). pp. 3–19 (2018)
40. Yang, Y., Soatto, S.: Fda: Fourier domain adaptation for semantic segmentation. In: Proceedings of the IEEE/CVF Conference on Computer Vision and Pattern Recognition. pp. 4085–4095 (2020)
41. Yi, Z., Zhang, H., Tan, P., Gong, M.: Dualgan: Unsupervised dual learning for image-to-image translation. In: Proceedings of the IEEE international conference on computer vision. pp. 2849–2857 (2017)
42. Yu, F., Koltun, V.: Multi-scale context aggregation by dilated convolutions. *arXiv preprint arXiv:1511.07122* (2015)
43. Zellinger, W., Grubinger, T., Lughofer, E., Natschläger, T., Saminger-Platz, S.: Central moment discrepancy (cmd) for domain-invariant representation learning. *arXiv preprint arXiv:1702.08811* (2017)
44. Zhang, P., Zhang, B., Zhang, T., Chen, D., Wang, Y., Wen, F.: Prototypical pseudo label denoising and target structure learning for domain adaptive semantic segmentation. In: Proceedings of the IEEE/CVF Conference on Computer Vision and Pattern Recognition. pp. 12414–12424 (2021)
45. Zhang, Q., Zhang, J., Liu, W., Tao, D.: Category anchor-guided unsupervised domain adaptation for semantic segmentation. *Advances in Neural Information Processing Systems* **32** (2019)
46. Zhao, H., Shi, J., Qi, X., Wang, X., Jia, J.: Pyramid scene parsing network. In: Proceedings of the IEEE conference on computer vision and pattern recognition. pp. 2881–2890 (2017)
47. Zhu, J.Y., Park, T., Isola, P., Efros, A.A.: Unpaired image-to-image translation using cycle-consistent adversarial networks. In: Proceedings of the IEEE international conference on computer vision. pp. 2223–2232 (2017)

## 6 Appendix

In the following sections, we provide additional qualitative and quantitative results and explanations that elaborate more deeply the unique contribution of ProCST as a booster to generic UDA tasks. First, we discuss the qualitative differences between translated images using the full ProCST model and the ablation study models presented in Section 4.3. Moreover, we present a detailed comparison between ProCST SiT data and EPE [26] generated data that illustrates



content preservation in ProCST’s image translation. This property is crucial for narrowing the domain gap between source and target domains in terms of UDA segmentation accuracy, as can be seen from the qualitative results presented in the paper. Finally, we present more examples for SiT and TiS translated images, generated using both source datasets (i.e. GTA5 and Synthia).

### 6.1 Ablation Study - Qualitative Results

The following section discusses the differences and similarities between GTA5  $\rightarrow$  Cityscapes translated images generated from three different ProCST ablation models: full ProCST model, ProCST model trained with no label loss (i.e.  $\lambda_{labels} = 0$ ), and ProCST model trained with only one scale (i.e.  $N = 1$ ). The quantitative results of all three models appear in Section 4.3.

Figures 6, 7, 8 and 9 present the original GTA5 image and all other SiT images generated using the compared models. Clearly, all three models create cloudy and green atmosphere as can be seen from Figure 6. This property matches Cityscapes domain. Yet, in figures 7, 8 and 9 we can see visually that



Fig. 6: Ablation Study. Top Left: original image; Top Right: ProCST full model; Bottom Left: ProCST with  $\lambda_{labels} = 0$ ; Bottom Right: ProCST model  $N = 1$ .

the full ProCST model adapts to the Cityscapes domain better than all other model. Visual quality, textures and general appearance are superior.

Images 8 and 9 show that the ablated models fail to generate good SiT images when dealing with complicated texture translations, like the smoothness of the road. Moreover, we can see that the quality of both ablated models is consistent with the quantitative results presented in the paper. While both variants are



Fig. 7: Ablation Study. Top Left: original image; Top Right: ProCST full model; Bottom Left: ProCST with  $\lambda_{labels} = 0$ ; Bottom Right: ProCST with  $N = 1$ .

comparable in the results, we can see some minor differences between the ProCST model trained without the label loss term (i.e.  $\lambda_{labels} = 0$ ) and the one trained without multiscale structure (i.e.  $N = 1$ ). Multiscale structure helps to translate complicated textures, as we can see for example from the road’s texture. Road is smoother and with deeper colors in the model with  $\lambda_{labels} = 0$  compared to the one with  $N = 1$ . Despite this fact, the first model sometimes suffers from artifacts that the latter does not. We can see such a trend in Figure 10. In the first row, observe the smoothness of the road and the deep green color that has superior quality in  $\lambda_{labels} = 0$  than  $N = 1$ . Yet, in the second row, the sky of the  $N = 1$  model is natural and clean while the sky of  $\lambda_{labels} = 0$  suffers from minor artifacts.



Fig. 8: Ablation Study. Top Left: original image; Top Right: ProCST full model; Bottom Left: ProCST with  $\lambda_{labels} = 0$ ; Bottom Right: ProCST with  $N = 1$ .



Fig. 9: Ablation Study. Top Left: original image; Top Right: ProCST full model; Bottom Left: ProCST with  $\lambda_{labels} = 0$ ; Bottom Right: ProCST with  $N = 1$ .





Fig. 10: Ablation Study. Left: ProCST with  $\lambda_{labels} = 0$ ; Right: ProCST with  $N = 1$ .

## 6.2 Comparison of ProCST and EPE [26]

We turn to present more comparisons between ProCST and EPE. Figure 11 presents more examples for objects that EPE’s translation deletes or distorts, while ProCST’s translation preserves. Figure 11 shows that trees in the sky are sometimes distorted due to the EPE translation. Note that these examples imply a more general trend. The EPE image translation is focused on generating good visual image quality, but not on preserving the content of the image. Thus, it sometimes distorts objects that do not visually fit their close spatial space. For example, the long palm trees are not consistent with their spatial environment (i.e. sky) and thus distorted.

We can see such a trend also in other cases. For example, in Figure 12, we can see a crop from the original source image that contains a sidewalk surrounded by vegetation. While the EPE translation distorts the sidewalk because of the vegetation from both of its sides, the ProCST model preserves the content and results in a cleaner image that has matching content to that of the original source image.

Content preservation is a crucial property in image translation when used for domain adaptation. EPE fails to achieve this property, and thus achieves poorer performance when employed as a booster to the UDA semantic segmentation task.



Fig. 11: Content Preservation. Left to right: Original source image; EPE translated image; ProCST translated image. ProCST’s output results in a clean image while EPE [26] distorts the palm trees due to the surrounding sky.



Fig. 12: Content Preservation. Top row: original source image; Bottom row from left to right: Crop taken from the original image; Crop taken from EPE translated image; Crop taken from ProCST translated image. ProCST’s output results in a clean image while EPE [26] distorts the sidewalk due to the surrounding vegetation.

### 6.3 SiT and TiS Translation Examples

We turn to provide additional examples of SiT and TiS images side by side with the original source images, for both source domains. Figure 13 shows GTA5  $\leftrightarrow$  Cityscapes translations and Figure 14 shows Synthia  $\leftrightarrow$  Cityscapes translations.



Fig. 13: Bi-directional GTA5  $\leftrightarrow$  Cityscapes image translation. Left to right: GTA5, SiT, Cityscapes, and TiS.



Fig. 14: Bi-directional Synthia  $\leftrightarrow$  Cityscapes image translation. Left to right: Synthia, SiT, Cityscapes, and TiS images.